Extended Abstracts of the 2009 International Conference on Solid State Devices and Materials, Sendai, 2009, pp250-251

J-2-4(Invited)

Performance Projections of III-V and Ge Channel MOSFETs

Hideaki Tsuchiya, Akihiro Maenaka, Takashi Mori, Yūsuke Azuma

Kobe University, Graduate School of Eng., Dept. of Electrical and Electronics Eng.
1-1, Rokko-dai, Nada-ku, Kobe 657-8501, Japan
Phone & Fax (common): +81-78-803-6082 E-mail: tsuchiya@eedept.kobe-u.ac.jp

1. Introduction

The remarkable advancement of integrated circuit technology has been primarily based on the downsizing of MOSFETs. But, in the present post-scaling era, the downsizing is not becoming an effective way to improve the device performance, because we have to meet all the requirements for suppressing leakage current, minimizing short channel effects and maintaining high drive current concurrently. Under such circumstances, the application of high mobility channel materials such as III-V semiconductors and Ge to *n*-MOSFETs is highly expected to achieve a better performance without downsizing [1].

To clarify advantages when the high mobility channels are introduced into practical MOSFETs, we have developed a quantum-corrected Monte Carlo device simulator (MONAQO), which considers material bandstructure, scattering processes and quantization in the inversion layer [2,3]. In this paper, we present performance projections of high mobility channel MOSFETs based on the simulator, and discuss their advantages over the Si-based MOSFETs.

2. Simulation Model

Table 1 shows the band parameters used in the simulation. It is well known that in high mobility III-V materials and Ge, an electron transfer to the higher valleys with a heavier transport mass degrades the device performance significantly [1]. The device structure is shown in Fig. 1, where we employ an ultrathin-body (UTB) structure with T_{Si}=5nm, to prevent a broadening of the inversion-layer electrons [2,3]. Ge (111) surface orientation [1,2,3] and the strained-Si channels under biaxially and uniaxially tensile strains with 1% are also considered. The effective mass reduction due to uniaxial tensile strain was taken into account based on the first-principles bandstructure calculation [4]. We considered impurity and phonon scatterings in the simulation, while roughness and electron-electron scatterings are ignored, to evaluate the intrinsic device performance of each material. Here, we should pay attention to the S/D donor concentration in III-V MOSFETs. Namely, the solid solubility of donors in III-V semiconductors is limited to be less than or comparable to 2×10^{19} cm^{-3} [5]. So, we assigned $N_D=2\times10^{19}$ cm^{-3} for GaAs and InP, and a higher $N_D=1\times10^{20}$ cm^{-3} for Si and Ge.

3. Ge UTB-MOSFETs

We first investigate the current drive of Ge UTB-MOSFETs. In Ge devices, L → X electron transition due to the phonon scattering greatly influences the electron transport [3]. As shown in Fig. 2, the electron population in the higher X valleys increases due to the L → X transition not only occurred in the channel, but also occurred in the source. Therefore, the drain current decreases significantly by those L → X transitions as shown in Fig. 3 (a). However, as the channel length decreases down to 20nm, the current reduction due to the L → X transition inside the channel is suppressed because of quasi-ballistic transport, and then an appreciably higher current drive than the Si UTB-MOSFET is obtained as shown in Fig. 3 (b). Consequently, the Ge (111) MOSFET exhibits substantially higher current drive than the Si-based MOSFETs at the ballistic limit as shown in Fig. 4, which is attributed to the smaller transport effective mass in the Ge (111) surface [1]. It is also found in Fig. 4 that uniaxially tensile strained-Si is one of the promising candidates for high mobility channels.

4. III-V UTB-MOSFETs

Next, we investigate III-V UTB-MOSFETs. Fig. 5 shows the channel length dependences of I_{ON} for all channel materials at (a) V_G=0.6V and (b) 1.0V. It is found that the current enhancement due to the ballistic transport is more effective in the group IV materials. In other words, the III-V MOSFETs are already quasi-ballistic in the sub-100nm channel lengths, so the advantage of the III-V materials becomes smaller toward the ballistic limit.

Here, we should point out that the increased parasitic resistance owing to the smaller S/D donor concentration limits the performance enhancement of III-V MOSFETs. As shown in Fig. 6 (d), a large potential drop is observed in the S/D regions of GaAs-MOSFETs, especially in the drain region, and thus the channel electrical field becomes lower. Then, we performed probatively a fictitious S/D with $N_D=1\times10^{20}$ cm^{-3} for the present III-V MOSFETs. By introducing such a heavily doped S/D, the electron averaged velocity increases due to the enhanced channel field and in addition, a higher sheet electron density is expected as shown in Fig. 7. As a result, the current drive of III-V MOSFETs drastically increases to ensure its advantage even at the ballistic limit, as shown in Fig. 8. Therefore, a lower resistive S/D such as metal S/D is needed to show its own real abilities of III-V materials.

5. Conclusions

The III-V MOSFETs, which are already quasi-ballistic in sub-100nm regime, lose their advantages over Si and Ge MOSFETs near the ballistic limit. A lower resistive S/D technology will be indispensable in practical use of ultrashort channel III-V MOSFETs.

References [1] S. Takagi et al., IEEE TED-55 (2008) 21. [2] T. Mori et al., IEEE TNANO-7 (2008) 237. [3] Y. Azuma et al., Phys. Stat. Sol. (c) 5 (2008) 3153. [4] T. Maegawa et al., IEEE TED-56 (2009) 553. [5] M. Fischetti et al., IEEE TED-38 (1991) 650.

		Si	Ge	GaAs	InP
mobility ($cm^2V^{-1}s^{-1}$)		1600	3900	9200	5400
mass (Γ)		–	0.037	0.067	0.082
mass (X)	m_t (m_0)	0.19	0.29	–	–
	m_l (m_0)	0.98	1.35	–	–
mass (L)	m_t (m_0)	–	0.082	0.127	0.153
	m_l (m_0)	–	1.59	1.538	1.878
nonparabolicity α		0.5 (X)	0.65 (L, Γ, X)	0.61 (Γ) 0.46 (L)	0.61 (Γ) 0.49 (L)
$\Delta E_{\Gamma L}$ (eV)		–	–	0.33	1.492
$\Delta E_{L\Gamma}$ / ΔE_{LX} (eV)		–	0.14 / 0.18	–	–
permittivity ε_r		11.9	16.0	12.9	12.6
E_f of S/D (eV)		0.064	0.138	0.278	0.326

Table 1 Effective masses, valleys and the other band parameters used in the simulation. Note that Fermi energies in III-V materials are a few hundreds meV, which is much higher than that of Si.

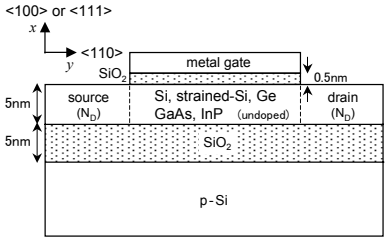

Fig. 1 Device model used in the simulation, where UTB structure and intrinsic channel are employed.

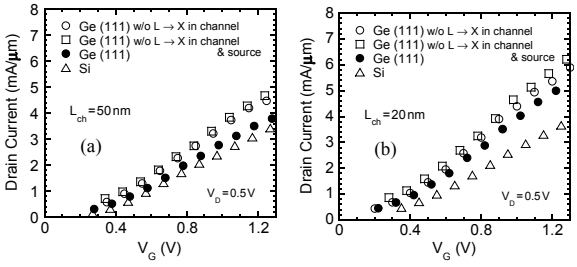

Fig.3 I_D-V_G characteristics for Ge (111)-UTB MOSFETs with (a) L_{ch}=50nm and (b) L_{ch}=20nm. V_{th} is set at 0.3V. The influences due to L → X scattering in the channel and source, and the results for Si-MOSFETs are also plotted.

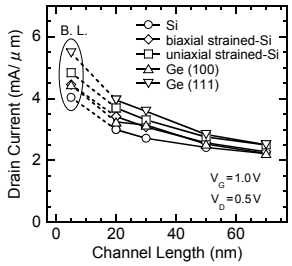

Fig.4 L_{ch} dependences of I_{ON} for Ge- and Si-based UTB-MOSFETs. The ballistic limit data are plotted as B. L.

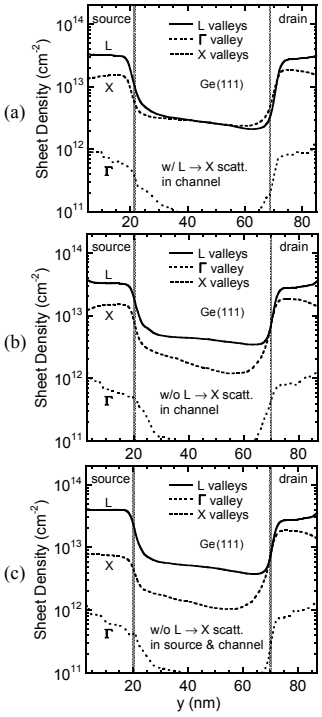

Fig.2 Sheet electron density for Ge (111)-UTB MOSFET at V_G=0.6V and V_D=0.5V. (a) with and (b) without L → X scattering in the channel, and (c) also without L → X scattering in the source.

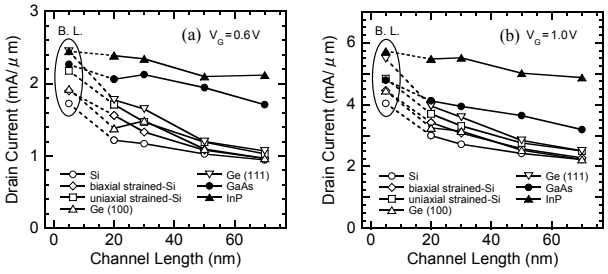

Fig.5 L_{ch} dependences of I_{ON} computed for all channel materials at (a) V_G=0.6V and (b) 1.0V. V_D=0.5V and V_{th}=0.3V. The degradation of GaAs channel at V_G=1.0V is owing to the Gunn effect.

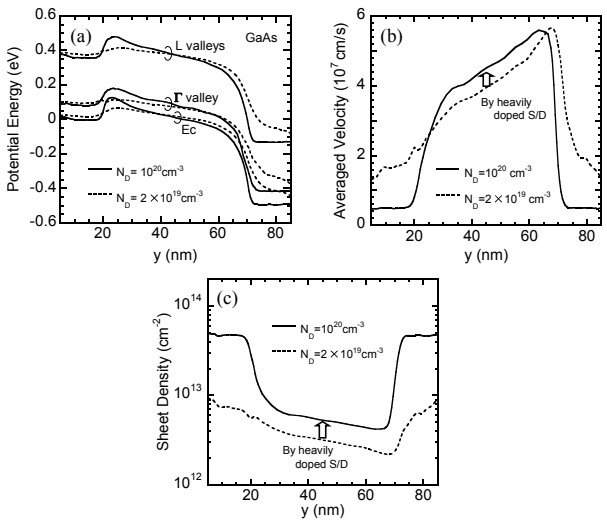

Fig.7 Improvement of transport properties in (a) potential profile, (b) averaged carrier velocity and (c) sheet carrier density due to heavily doped S/D in GaAs-MOSFET.

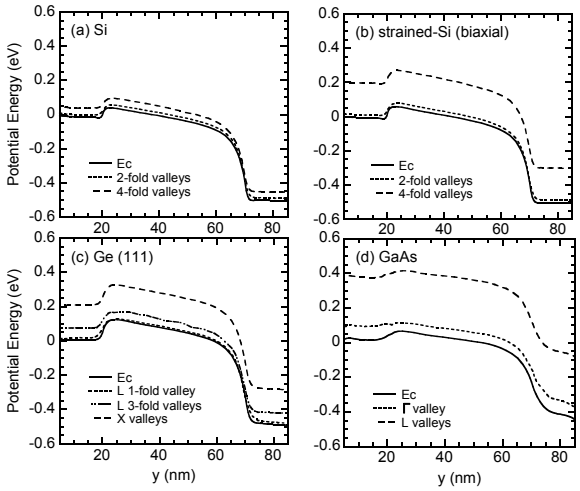

Fig.6 Potential energy profiles for each valley in (a) Si, (b) biaxial strained-Si, (c) Ge (111) and (d) GaAs channels, where V_G=0.6V and V_D=0.5V. Note that quantum potentials are included and thus the lowest valley is located above the conduction band-edge E_c.

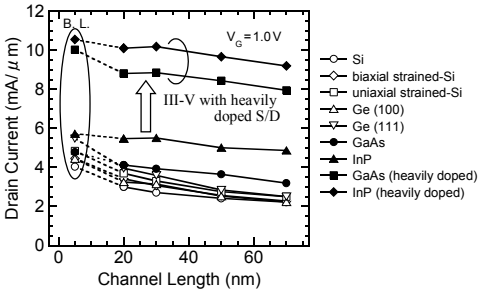

Fig.8 Drive current enhancement due to heavily doped source and drain in III-V MOSFETs. V_G=1.0V and V_D=0.5V. V_{th}=0.3V.